Journal of Thermal Science Vol.21, No.3 (2012) 197−208

DOI: 10.1007/s11630-012-0536-3 **Article ID: 1003-2169(2012)03-0197-12**

Investigation of the Flow in the Impeller Side Clearances of a Centrifugal Pump with Volute Casing

Björn-Christian Will, Friedrich-Karl Benra and Hans-Josef Dohmen

Institute of Energy and Environmental Engineering, Turbomachinery, University Duisburg-Essen, 47048 Duisburg, Germany

The paper is concerned with the fluid flow in the impeller side clearances of a centrifugal pump with volute casing. The flow conditions in these small axial gaps are of significant importance for a number of effects such as disk friction, leakage losses or hydraulic axial thrust to name but a few. In the investigated single stage pump, the flow pattern in the volute turns out to be asymmetric even at design flow rate. To gain a detailed insight into the flow structure, numerical simulations of the complete pump including the impeller side clearances are accomplished. Additionally, the hydraulic head and the radial pressure distributions in the impeller side clearances are measured and compared with the numerical results. Two configurations of the impeller, either with or without balancing holes, are examined. Moreover, three different operating points, i.e.: design point, part load or overload conditions are considered. In addition, analytical calculations are accomplished to determine the pressure distributions in the impeller side clearances. If accurate boundary conditions are available, the 1D flow models used in this paper can provide reasonable results for the radial static pressure distribution in the impeller side clearances. Furthermore, a counter rotating wake region develops in the rear impeller side clearances in absence of balancing holes which severely affects the inflow and outflow conditions of the cavity in circumferential direction.

Keywords: Cavity, Rotor-Stator Cavities, Side Chambers, Centrifugal Pump

Introduction

Cavity flows are encountered in nearly all kinds of fluid machines. For example, the efficiency of a centrifugal pump is essentially influenced by the flow in the side chambers. Disk friction and volumetric losses are dominant especially in low specific speed pumps. Furthermore, the pressure increase in the impeller causes hydraulic forces on the rotor which determine the bearing design. The radial load on the impeller depends on the pressure distribution in circumferential direction. Axial thrust is mainly determined by the radial pressure distribution in the side cavities. Commonly, a leakage flow passes the cavities caused by the pressure difference across the impeller. In the present study, two impeller configurations of a centrifugal pump with volute casing are investigated and compared. First, the impeller is equipped with balancing holes (b.h.) to compensate, respectively reduce, the resulting axial thrust. Consequently, the leakage is directed centripetally inwards in the rear-side chamber. Second, the holes are closed to avoid a radial through-flow.

The principal flow structure in a rotor-stator cavity can be described as follows: Due to viscosity, the fluid in the cavity is set into motion by the rotation of the impeller. The no-slip condition requires that the fluid matches the

Received: December 2011
Björn-Christian Will: Dipl.-Ing.

Nomenclature

$\beta=\omega/\Omega$	Core rotation coefficient	$\tau_0, \tau_0^{\varphi}, \tau_0^{r},$	Total, tangential and radial wall shear stress
$G=s/b$	Dimensionless gap size	v_{mean}	Mean velocity
$\mathrm{Re}_{\varphi}=\frac{\Omega\cdot b^2}{\nu}$	Circumferential Reynolds number	α	Angle between shear stress at the wall and the tangential direction
a	Hub radius	A, B	Constants
b	Outer impeller radius	$\mathrm{Re}_l=\frac{\Omega\cdot r^2}{\nu}$	Local Reynolds number
l_1, l_2	Radial gap heights	v_{rR},v_{rs}	Radial velocity (rotor, stator b.l.)
s	Axial gap width	z_R, z_S	Axial coordinates (positive from the rotor and stator wall)
Ω	Angular speed of the rotor	a, a*	Velocity factors
$\overline{r}=r/b$	Dimensionless radius	n, m	Exponents for velocity profiles
$\varphi_G=\frac{Q}{\pi\cdot\Omega\cdot b^3}$	Dimensionless through-flow rate	C_1	Constant
Q	Volume flow rate	f	Correction function
		n_q	Specific speed of the pump
λ_R, λ_S	Friction factors (rotor, stator)	φ	Perimeter coordinate
ω	Angular velocity of the fluid	H	Delivery head
δ_R, δ_S	Boundary layer thickness (rotor and stator)	p_{tot}	Total pressure
Re_R, Re_S	Reynolds number for the rotor and stator boundary layer	p	Pressure
ν	Kinematic viscosity	$p^*=\frac{2\cdot p}{\rho\Omega^2 b^2}$	Dimensionless pressure
C_{fmean}	Friction coefficient	β_e	Boundary values for the core rotation
ρ	Fluid density	p_e	Boundary value for the pressure

circumferential velocity at the rotating wall and is at rest at the stationary wall. For a "wide gap" an intermediate velocity established between the walls referred to as "core region". The circumferential velocity in the core is generally characterized by the core rotation coefficient β, defined as the ratio of the angular velocity of the fluid to the angular velocity of the impeller. Due to the dominant tangential motion, a radial pressure gradient results, with its maximum value at the outer radius of the cavity.

In the core, centrifugal and pressure forces balance each other with no occurance of any other forces (radial equilibrium). At the stationary wall (Bödewald layer) the tangential velocity is reduced to zero and therefore radial inflow develops. This centripetal motion is caused by the pressure imposed on the boundary layer from the core region. Centrifugal forces near the rotor surface (Ekman layer) lead to radial outflow.

According to [2], the flow structure for an enclosed rotating disk (no leakage) can be divided into four regimes in dependence on the dimensionless gap size G and the circumferential Reynolds number Re_{φ}:

Regime I: Small clearance, laminar flow
Regime II: Large clearance, laminar flow
Regime III: Small clearance, turbulent flow
Regime IV: Large clearance, turbulent flow

The boundary layers can either be merged or not, and the flow can be laminar or turbulent. For flow regimes II or IV, which are supposed to apply in the majority of practical applications ([4] [5]), the basic structure is indicated in Fig.1 (see also [6]): A boundary layer on rotor (IV) and stator (I), a core region (III) and an intermediate layer (II) between stator boundary layer and core with a small radial outflow. Due to mass conservation, an axial convection of fluid from the stator to the rotor takes place which is important for the overall transport of angular momentum.

The circumferential velocity distribution in the core region essentially dictates the pressure distribution and frictional resistance of the rotor. The torque is affected by the circumferential velocity gradient in axial direction while the pressure is determined by the magnitude of the circumferential velocity. In centrifugal pumps, the

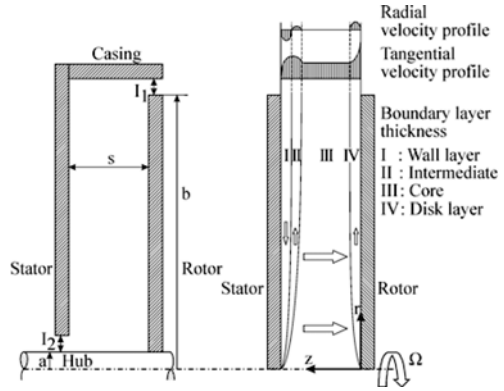

Fig. 1 Idealized cavity geometry (left) and principal flow structure (right)

pressure in the impeller side clearances decreases with decreasing radial coordinate depending on the core rotation.

According to [7], the frictional resistance of the rotor is determined by the angular momentum flux difference between the radial outward flow and the axial inward flow in the rotor boundary layer. The axial inward flow in the rotor boundary layer carries angular momentum with it and therefore the torque for an enclosed rotating disk is significantly smaller than for a free disk.

In general, a leakage flow passes the cavities which can be oriented in centrifugal (hub to casing) or centripetal (casing to hub) direction. The fluid leaving the impeller can contain a considerable amount of angular momentum. Generally, the angular momentum flux entering the impeller side clearances is the most important parameter with respect to the radial pressure distribution and the frictional resistance of the impeller.

Analytical Flow Model

In the following, a new 1D flow model is presented under assumption of flow regime IV with separate boundary layers. A simplified differential equation for the radial gradient of the core rotation can be deduced from the tangential momentum equation assuming steady, axisymmetric flow with no body forces. Using the integral boundary layer theory, the final equation yields [8]:

$$\frac{d\beta}{d\bar{r}} = \frac{\bar{r}^2}{4\varphi_G}\left(\lambda_S\beta^2 - \lambda_R\left(1-\beta\right)^2\right) - \frac{2\beta}{\bar{r}} \tag{1}$$

Considering the friction factors (λ_S, λ_R) as equal in equation (1), the fluid would rotate with half the angular speed of the rotor in case of zero leakage (solid body rotation). For infinite leakage, the radial distribution of the core rotation takes the form of a potential swirl ($b\cdot\bar{r}^2 = const.$) known as inviscid solution.

For a further evaluation, the friction factors need to be specified. In general, the empirical correlation according to Blasius is adopted which is limited to a certain Reynolds number range [9].A novel approach based on the universal logarithmic law of the wall is employed.

Prandtl derives a friction law which agrees very well with available experimental data over the entire range of turbulent Reynolds numbers [9]:

$$\frac{1}{\sqrt{\lambda}} = 2\lg\left(\mathrm{Re}\sqrt{\lambda}\right) - 0.8 \tag{2}$$

To apply this correlation to cavity flow, the Reynolds numbers for rotor and stator are defined as:

$$\mathrm{Re}_R = \frac{\left(\Omega-\omega\right)r2\delta_R}{\nu} \tag{3}$$

$$\mathrm{Re}_S = \frac{\omega r2\delta_S}{\nu} \tag{4}$$

Next, information about the radial evolution of the boundary layer thicknesses is necessary. The rotor friction coefficient C_f can be expressed by Dean's formula according to [10]:

$$C_{fmean} = 0.073\,\mathrm{Re}_R^{-\frac{1}{4}} \tag{5}$$

The original formula is adapted to the present problem by replacing the mean Reynolds number with equation (3). The friction coefficient and thus the effective shear stress become:

$$C_{fmean} = \frac{\tau_0}{\frac{\rho}{2}v_{mean}^2} \sim \left(2\Omega r\left(1-\beta\right)\right)^{-\frac{1}{4}}\left(\frac{\delta_R}{\nu}\right)^{-\frac{1}{4}} \tag{6}$$

Due to the cross-flow component, the total wall shear stress is composed of a radial and a tangential component. The tangential wall shear stress can be written using the angle α as:

$$\tau_0^{\varphi} = \tau_0\cos\alpha \sim \rho\left(2\Omega r\left(1-\beta\right)\right)^{\frac{7}{4}}\left(\frac{\nu}{\delta_R}\right)^{\frac{1}{4}} \tag{7}$$

The radial wall shear stress is in equilibrium with the centrifugal force in a volume element with the height δ_R.

$$\tau_0^r = \tau_0\sin\alpha = \rho\Omega^2 r\delta_R \tag{8}$$

Equating (7) and (8) eliminates the shear stresses and results in a general expression for the boundary layer thickness on the rotor:

$$\delta_R = A\frac{r}{\mathrm{Re}_l^{\frac{1}{5}}}\left(1-\beta\right)^{\frac{1}{5}} \tag{9}$$

This equation resembles the experimental relation proposed by [3] which is used, for example, with slight modifications in the exponent n and the constant B in the flow models given in [11], [12]:

$$\delta_R = B\frac{r}{\mathrm{Re}_l^{\frac{1}{5}}}\left(1-\beta\right)^{n} \tag{10}$$

The proportionality constant A can be determined for example by comparison with the results of [13]. A value of A=0.3035 is adopted in the present study. As already briefly discussed in the description of the general flow structure, the boundary layer thickness of the disk decreases for increasing Reynolds numbers according to equation (9) and agrees with the principal relations found by [2]. Thus, for high Reynolds numbers, a flow structure with separated boundary layers can be expected.

A relation for the stator boundary layer thickness can be obtained from the continuity equation. The relation formulates under assumption of zero radial velocity in the core:

$$\int_0^{\delta_S} v_{rS}\,dz_S + \int_0^{\delta_R} v_{rR}\,dz_R = \frac{Q}{2\pi r} \tag{11}$$

The following profiles are assumed for the radial velocity components in the rotor and the stator boundary layer according to [12]:

$$v_{rS} = -\alpha\beta r\Omega\left(1-\frac{z_S}{\delta_s}\right)^n \cdot \left(\frac{z_s}{\delta_s}\right)^{\frac{1}{m}} \tag{12}$$

$$v_{rR} = \alpha^*(1-\beta) r\Omega\left(1-\frac{z_R}{\delta_R}\right)^n \cdot \left(\frac{z_R}{\delta_R}\right)^{\frac{1}{m}} \tag{13}$$

In this study, n=2 and m=7 are chosen. The velocity factors a and a* can be determined from the empirical relations given by [12] based on flow angle measurements for flow regime IV:

$$a = 1.03\left(\frac{\mathrm{Re}_l}{10^5}+2\right)^{-0.387} \tag{14}$$

$$a^* = 1.18\left(\frac{\mathrm{Re}_l}{10^5}+2\right)^{-0.49} \tag{15}$$

Several different formulations for the velocity profiles can be found in the literatures (e.g. [2], [11], [12]) which basically differ in the form function chosen. Introducing these profiles in the continuity equation and solving for the stator boundary layer thickness gives:

$$\delta_S = A\frac{a}{a^*}\frac{(1-\beta)^{\frac{12}{5}}}{\beta}\frac{r}{\mathrm{Re}_l^{0.2}} - \frac{\varphi_G}{\beta}\frac{b}{2aC_1\bar{r}^2} \tag{16}$$

The value for the constant C_1 depends uniquely on the form function and amounts to C_1=0.408 in the present case. For centripetal flow, the volume flow rate is negative and therefore the stator boundary layer thickness increases because the flow passes the cavity close to the stator. The thickening of the Bödewald layer in case of radial inward flow is also noticed in the numerical study of [14].

Tests with the flow model in its original form indicate a slightly excessive increase in the core rotation in case of low entrance rotation and large axial gap widths. The decelerating effect of an outer radial shroud (casing in Fig. 1) on the core rotation has not yet been accounted for in the present formulation. The overall decelerating influence of a stationary shroud on the core rotation is obvious in case of an enclosed rotating disk. Usually, measured as well as computed values are below the theoretical maximum of 0.5 valid for infinite disks. If a centripetal through-flow is present, the shear stress created by the interaction of the entering leakage with the shroud gives rise to an additional "dynamic stress" whose influence diminishes for decreasing radial locations. To include both effects in the flow model, a correction function f for the resistance factor of the stator is introduced.

$$\frac{d\beta}{d\bar{r}} = \frac{\bar{r}^2}{4\varphi_{Sp}}\left(f\cdot\lambda_S\beta^2 - \lambda_R(1-\beta)^2\right) - \frac{2\beta}{\bar{r}} \tag{17}$$

The function f is defined as follows:

$$f = 1+\left(\frac{s}{b+l_1-a}+5\bar{r}^4\left|1-\frac{\beta}{0.58}\right|^{\frac{6}{5}}\right) \tag{18}$$

The first term in the correction function can be considered as a static influence. The second term accounts for the dynamic influence resulting from interaction of the shroud with the leakage flow whose influence is confined to the outer radii.

A fourth order Runge-Kutta method has been employed for the solution of equation (17), as well as for all other analytical models used in this paper. The friction factors are determined using an iterative calculation procedure known from pipe flow calculations for each radial position.

The flow model has been compared to the experimental data obtained by [15] who examines the flow in the impeller side gap with special attention to the influence of the cavity anteroom. In the experiments, the radial core rotation distribution is measured using Laser-Doppler Anemometry. These results are used for comparison because the non-invasive technique does not disturb the flow. It is noted by [4] that several authors encountered systematic deviations between the integrated measured radial velocity profiles and the separately measured volume flow rate (e.g. [16]) when using velocity probes. The comparisons for the plane rotor-stator cavity incorporate different leakage flow rates, gap widths and entrance rotation values as they typically occur in centrifugal pumps. For comparison purposes, the calculated curves from the flow models of [17] and [12] are additionally included. The proposed model gives good results. Especially at the outer radius the modified flow model improves the prediction with respect to the experimental values over the entire range of investigated parameters (see Fig.2). The outer disk regions are of predominant importance for the prediction of disk friction and axial thrust.

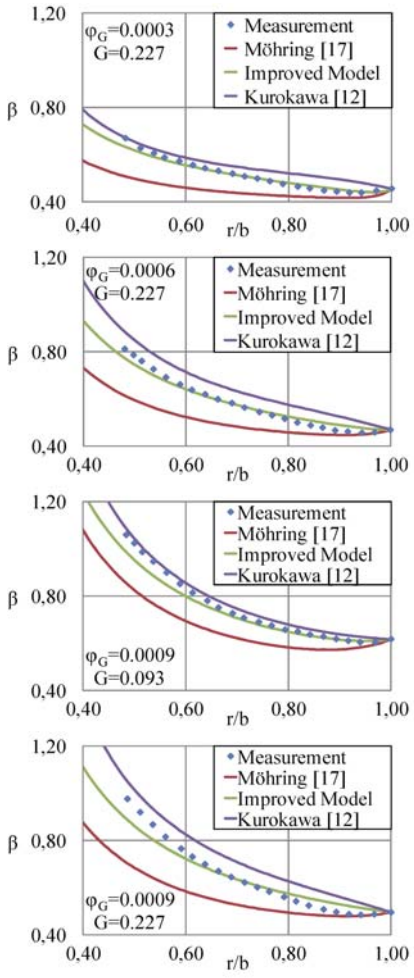

Fig. 2 Comparison between calculated and measured distributions of the core rotation coefficient

Investigated Pump

The centrifugal pump under investigation is a commercial standard pump in compliance with the guidelines of the International Organization for Standardization (ISO). The specific speed is n_q=22.8min$^{-1,}$ for which impellers with relatively large radial extent are common, causing high disk friction and leakage losses. The impeller is shrouded and has seven three-dimensional, strongly backward curved blades. The flow leaving the impeller is collected by a volute casing. The main data are summarized in Table 1.

To reduce the axial force, the impeller has seven balancing holes, one in each blade passage. This leads to a radial inward directed flow in both impeller side clearances. In the second configuration, the balancing holes are closed.

Numerical Model

Transient, fully 3D computations solving the Reynolds-averaged Navier-Stokes equations using the commercial CFD code Ansys CFX 12 are conducted in order to predict the flow in the whole pump including both impeller side clearances. A block structured mesh with an overall amount of more than 12 million cells is used. The y^+ magnitudes at all walls in the flow domain are below 30. Fig.3 shows two cross sectional views of the computational mesh in an axial and in the meridional plane.

Table 1 Main data of the pump

Impeller	
Number of blades	7
Outlet width	14 mm
Outlet radius	130 mm
Number of balancing holes	7
Diameter of the balancing holes	5.5 mm
Volute casing	
Basic circle radius	140 mm
Volute width at the basic circle	25 mm
Design operating conditions	
Volume flow rate	80 m^3/h
Speed of rotation	1450 min^{-1}
Impeller side clearances	
Width of front impeller side clearances	7.57 mm
Width of rear impeller side clearances	3 mm

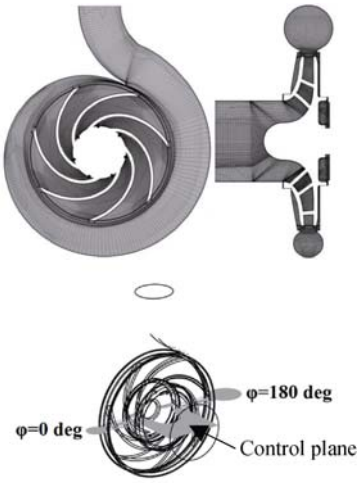

Fig. 3 Computational model and control plane

Close to the inlet radius of the impeller, the balancing holes are visible. In order to model turbulence, a k-ω SST model is applied which is considered as a good compromise between accuracy and computational effort even for the impeller side clearances [18]. At the inlet, the total pressure and the direction of the absolute velocity vector are specified while the mass flow rate at the outlet is given as a boundary condition. The no-slip condition is

applied at all wall boundaries in the relative frame of reference.

The numerical results obtained in this study are basically evaluated on the same perimeter coordinates as the experiments. In the lower part of Fig.3, a wireframe model of the pump including the control plane for the evaluation is shown using the angle φ as perimeter coordinate.

Experiments

In the present study, the pump is operated at design flow rate (80 m^3/h), part load (48 m^3/h) and overload (96 m^3/h). The hydraulic head is obtained from the total pressure difference by measuring the pressure at the inlet and the outlet of the pump:

$$H = \frac{p_{tot,outlet} - p_{tot,inlet}}{\rho g} \tag{19}$$

with the total pressure being the sum of the static and dynamic pressure:

$$p_{tot} = p + \frac{\rho}{2} v_{mean}^2 \tag{20}$$

In order to determine the radial pressure distribution in the impeller side clearances, static pressure measurements at different radial locations are conducted in both impeller side clearances by pressure holes in the casing wall. More details can be found in [1].

Results for the Design Point

A comparison of the hydraulic heads at design flow rate is given in Table 2. The balancing holes lead to a noticeable reduction of the hydraulic head due to increased losses.

Table 2 Comparison of hydraulic heads at design flow rate (Q=80m^3/h)

Exp. with balancing holes	18.5m
CFD with balancing holes	18.3m
Exp. without balancing holes	18.74m
CFD without balancing holes	19m

In the present case, the pressure in the volute casing increases in flow direction even at design flow rate. The reason is that the volute and the impeller are obviously designed for different flow rates. This causes a radial force on the impeller and variable flow conditions in the blade passagess during each rotation. As a consequence. the peripheral conditions of the impeller side clearances depend on the perimeter coordinate. The impeller side clearances in pumps with volute casing are relatively open at the outer radius, which leads to a strong coupling between the flow in the volute, the impeller outflow and the impeller side clearances. Consequently, the pressure in the cavities varies in circumferential direction too (see Fig.4, Fig.5).

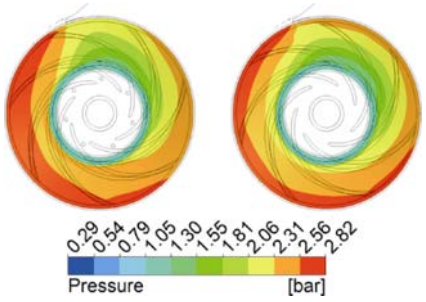

Fig. 4 Pressure distribution along the casing walls in the front impeller side clearances (left: impeller with balancing holes, right: impeller without balancing holes)

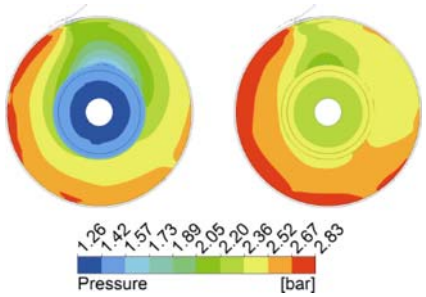

Fig. 5 Pressure distribution along the casing walls in the rear impeller side clearances (left: impeller with balancing holes, right: impeller without balancing holes)

A comparison with the measured radial pressure distributions on the casing walls in the respective impeller side clearances either with or without balancing holes in the impeller is given in the next diagrams (Fig.6, Fig.7).

The overall agreement between the measured and numerically predicted curves in the front impeller side clearances is very good in both cases.

The results confirm the expected decrease of the pressure towards the inner radii resulting from an increase in the core rotation caused by the inward angular momentum flux at the outer radius. According to the principle of conservation of angular momentum, the circumferential velocity must increase when the radius decreases. In case of inviscid flow, the velocity distribution would adjust according to the potential swirl ($v_\varphi \cdot r$=const.) distribution.

The pressure is imposed onto the boundary layers from the core region for flow regime IV and seems to be sufficiently captured with the present numerical set up.

In the front impeller side clearances, the static pressure distribution changes slightly for the two configurations. In absence of balancing holes, a stronger decrease of the pressure towards the axis of rotation can be observed which results from a stronger acceleration of the core flow in radial inward direction.

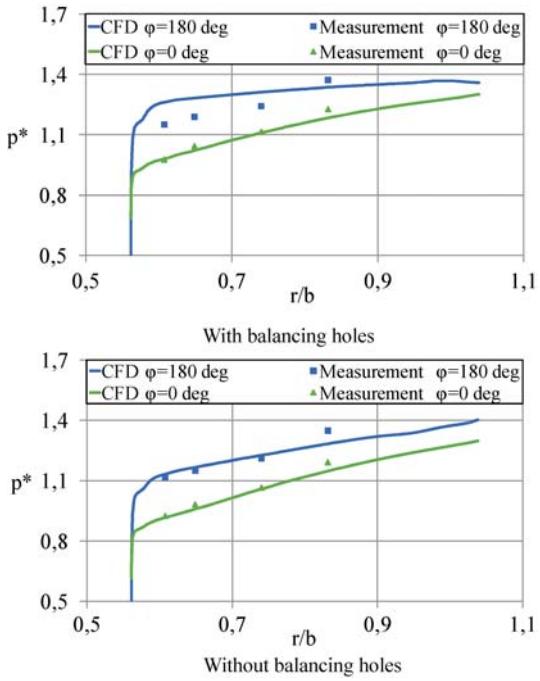

Fig. 6 Radial pressure distribution in the front impeller side clearances ($Q/Q_{opt}=1$)

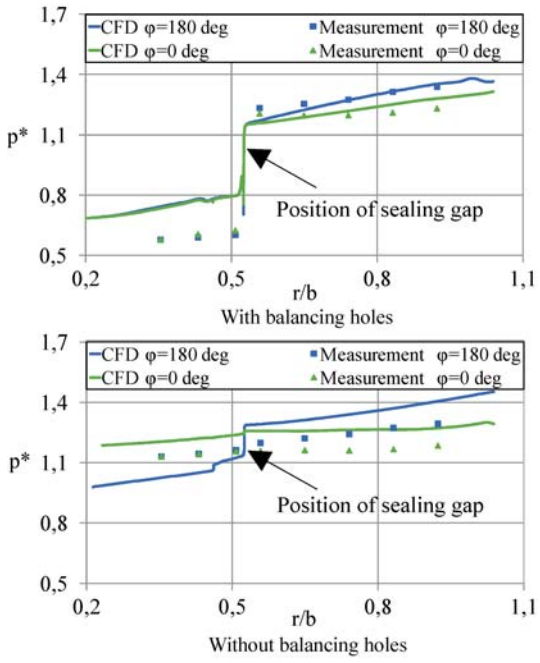

Fig. 7 Radial pressure distribution in the rear impeller side clearances ($Q/Q_{opt}=1$)

This is caused by an increased angular momentum flux entering at the outer radius as will be shown later on.

For the impeller with balancing holes, a centripetal inward directed leakage is present in the rear impeller side clearances too, and a considerable axial throughflow is present across the sealing gap. Somewhat larger discrepancies are apparent between the measured and computed values (Fig.7). However, a significantly smaller radial pressure gradient is present which can be explained by a change in the basic flow regime. Due to the very small axial distance, the boundary layers on the rotating and the stationary wall interact and the flow belongs to Regime III according to [2]. The influence of viscosity is not restricted to the near wall regions any more and extents throughout the complete axial gap. For this reason, the pressure distribution is strongly affected by the wall shear stress. The influence of the leakage flow is much weaker in the rear impeller side clearances compared to the front impeller side clearances.

For zero leakage in the rear impeller side clearances, the sealing gap has much less effect on the flow structure since the axial flow component diminishes. This can be clearly seen from the measurements and the CFD results.

A fundamental difference seems to be present in the radial evolution of the pressure at φ=180 deg compared to φ=0 deg in Fig.7 for the rear impeller side clearances. The shape of the blue curve indicates a non-negligible axial velocity across the gap although no general leakage flow is present because the balancing holes are closed. When the balancing holes are closed, a counter rotating wake region develops in the rear impeller side clearances at the tangential position φ=0 deg. The low static pressure after the tongue accelerates the fluid in tangential direction which cannot be counterbalanced by a radial pressure force, and as a result, a recirculation region develops. Obviously, this effect is directly related to the asymmetric pressure build up in the volute.

In the immediate vicinity of the rotating wall, the fluid rotates in the same direction as the rotor due to the dominant influence of the centrifugal forces. For farther wall distance, the influence of the pressure becomes stronger and recirculation develops. The strongest recirculation takes place in the vicinity of the casing wall.

Furthermore, the inflow and outflow in the rear impeller side clearances in tangential direction is highly non-uniform. After the wake, the fluid is centrifuged out of the cavity into the volute and mixes with the main flow. Just before the tongue, fluid is sucked into the impeller side clearances due to the pressure gradient in radial direction at this position. Exactly this fluid which is sucked into the impeller side clearances is responsible for the small pressure drop in Fig.7, since a part of this flow flows axially across the sealing gap. This can be seen from the 3D streamlines in Fig.8. In the wake region, the pressure remains relatively constant in radial direction. No similar effects are observed in the front impeller side clearances due to the much stronger inward directed leakage flow.

A pressure difference between the cavity inlet and the balancing holes superposes a radial flow component which suppresses the creation of a wake region by im-

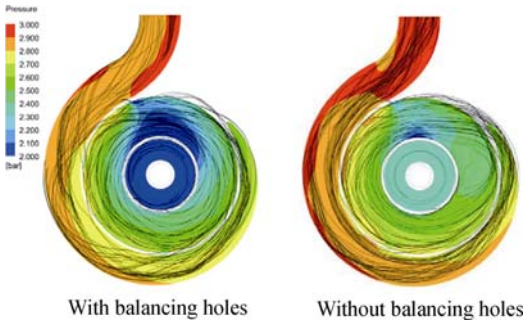

Fig. 8 3D streamlines and pressure contour at z/s=0.917

plying a spiral type inward motion. The appearance of the wake region has been confirmed for the part load point as well, whereas in case of overload (Q/Q_{opt}=1.2) the pressure asymmetry becomes significantly smaller, as well as the wake region. This confirms that the volute seems to be designed for higher flow rates. Inside the volute, fluid particles follow curved streamlines. Streamline curvature requires a pressure gradient normal to the flow direction causing secondary flows. Fig.9 shows simplified pictures of the velocity vectors for two locations at φ=0 deg and φ=180 deg and the two impeller configurations. The colors represent inflow (green) and outflow (red) in radial direction. First, it can be observed that the flow fields differ very much from each other according to the circumferential coordinate. The disk pumping effect is clearly visible for the impeller with balancing holes at φ=0 deg. The fluid pumped radially outward mixes with the main flow from the blade passages while a radial inflow takes place only in the vicinity of the stationary casing walls. This radial inflow results from the secondary flow in the volute and contains a lower circumferential velocity component compared to an inflow directly from the impeller. This causes higher disk friction and reduces the pressure drop across the cavity. A reduced rise of the circumferential velocity with decreasing radius results in a higher pressure force on the disk.

For closed balancing holes, the flow field shifts to the left, slightly reducing the inflow in the front impeller side clearances but increasing the interaction with the main flow from the impeller. This is caused by a pressure gradient in axial direction at the pump outer radius resulting from the pressure increase in the rear impeller side clearances due to the absence of leakage. The overall inward angular momentum flux in the front impeller side clearances increases by about 20% which can also be noticed from the stronger gradient of the pressure curve in Fig.6. Furthermore, a stronger interaction of the secondary flow in the volute with the recirculating flow in the rear impeller side clearances can now be observed which reduces the radial outflow on the disk.

The circumstances at φ=180 deg are different for the impeller with balancing holes. The higher pressure level causes a much stronger inflow into the impeller side clearances which reduces the radial outflow on the rotating surfaces. Once more, the shifting towards the suction side is clearly visible for the impeller without balancing holes. The leakage flow in the front impeller side clearances at this position is mainly fed from the impeller, confirming that the overall angular momentum flux must be higher.

Analytical calculations with the proposed flow model and a model developed by [12] for merged boundary layers have also been conducted for both impeller side clearances. In the case of flow regime IV, the pressure is calculated from the radial core rotation distribution using the assumption of radial equilibrium in the core region [8]. The necessary input parameters for the calculation are given in Table 3 and are evaluated from the numerical simulation (area averaged values at the outer cavity radius).

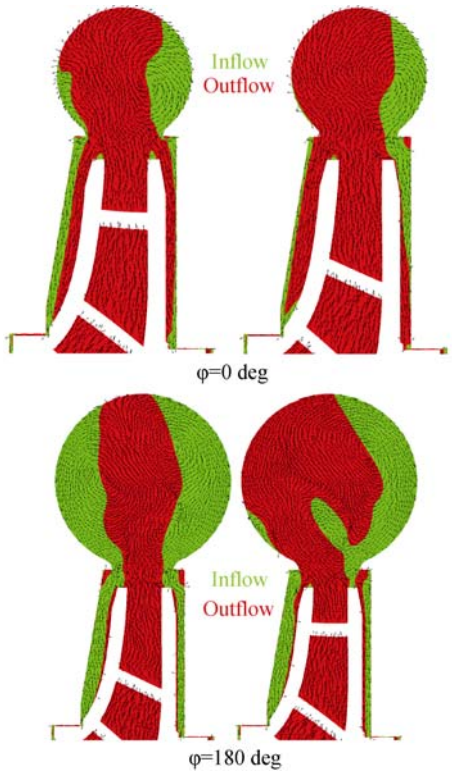

Fig. 9 Comparison of secondary flow patterns (left: impeller with b.h.(balancing holes), right: impeller without b.h.)

Table 3 Boundary conditions for analytical flow models

	φ_G	β_e	p_e [Pa]
Impeller with balancing holes			
Front impeller side clearances	0.001896	0.42	252737
Rear impeller side clearances	0.0006425	0.395	252528
Impeller without balancing holes			
Front impeller side clearances	0.00155	0.566	255263
Rear impeller side clearances	0	0.3975	262627

The comparison of the proposed flow model with the experimental data (Fig.10) for the front impeller side clearances, with respect to averaged values between φ=0 deg and φ=180 deg, shows a good agreement for both the case with balancing holes ("bh") or the case without balancing holes ("wbh"). In absence of through-flow, a very small leakage is used for the calculation because the numerical solution does not allow a value of zero. In the rear impeller side clearances, the agreement for the case with leakage is somewhat worse. This can be attributed to the overall higher pressure level predicted by the CFD simulation that is used to obtain the pressure at the cavity entrance. This pressure is necessary as boundary condition for the numerical determination of the radial pressure distribution using the flow model. If an entrance pressure extrapolated from the measurements is used ("Kurokawa merged bl wbh (2)"), the computed curve falls right between the measured points at φ=0 deg and φ=180 deg. The radial trends show that the influence of the inward angular momentum flux via the leakage flow has much less effect in the case of flow regime III compared to regime IV. The shape of the curve changes only slightly, while in the front impeller side clearances, the decrease of the pressure for lower radii is accompanied by a magnification of the core rotation.

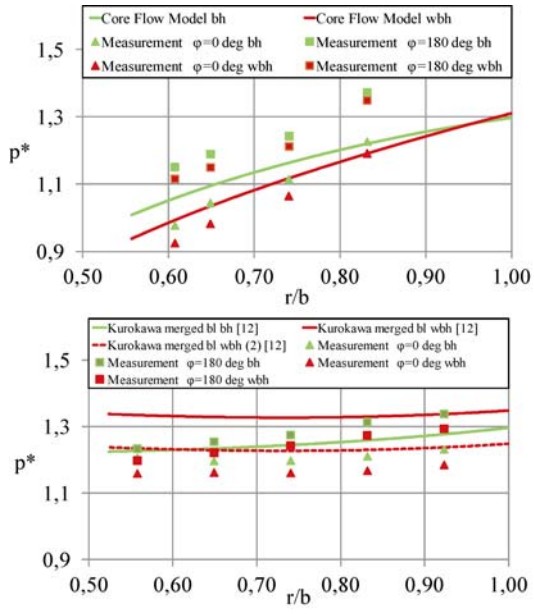

Fig. 10 Comparison between experimental results and analytical models (upper diagram: front impeller side clearances, lower diagram: rear impeller side clearances)

Results for Off-Design Conditions

In principle, the flow conditions at off-design operation are more complicated. As shown before, even at the design operating point a circumferential pressure gradient is present in the volute. The hydraulic heads obtained from the numerical simulation and the experiment for all three operating points are summarized in Table 4.

Table 4 Comparison of hydraulic heads

	Q/Q_{opt}=0.6	Q/Q_{opt}=1	Q/Q_{opt}=1.2
CFD bh	20.04m	18.3m	16.8m
Exp. bh	20.12m	18.5m	17.1m
CFD wbh	20.3m	19m	17.34m
Exp. wbh	20.16m	18.74m	17.54m

The agreement between the numerical and the experimental results for both impeller configurations is very good, the maximum deviation is less than 2%. For all investigated operating points, the efficiency reduction caused by the balancing holes is clearly visible. Generally, the pressure in the pump increases at part load and decreases at overload conditions. In the front impeller side clearances, the flow structure remains principally the same as at the design point. For the impeller without balancing holes, the pressure drop is consistently higher due to the increased amount of angular momentum entering the impeller side clearances. The angular momentum flux slightly decreases with increasing pump flow rate and is always higher for the impeller without balancing holes. The latter can also be seen from the slope of the pressure distribution compared to the impeller with balancing holes.

In the rear impeller side clearances, the decrease of the leakage flow rate with increasing pump flow rate is clearly visible from the resultant pressure drop across the sealing gap. A continuous reduction is apparent when the pump flow rate increases. From the pressure diagrams for part load and overload conditions (Fig.11, Fig.12, Fig.13, Fig.14), it can be concluded that the basic relationships remain the same as for design flow rate except that the overall pressure level varies according to the operating point.

According to Fig.13 and Fig.14, an appreciable reduction of the peripheral pressure difference between φ=0 deg and φ=180 deg is obvious. This indicates that the volute casing seems to be originally designed for a higher flow rate than the impeller. Also the pressure distributions for the overload point in case of closed balancing holes indicate that the wake region caused by the pressure asymmetry became smaller in size. The contrary prevails at the part load point where the size of the wake region increases. The secondary flow patterns confirm the presumption that the volute is designed for a higher flow rate because the secondary flow component is directed straight radially outwards at both control planes. Again, the same fundamental relations as for the design point apply. Closing of the balancing holes deflects the

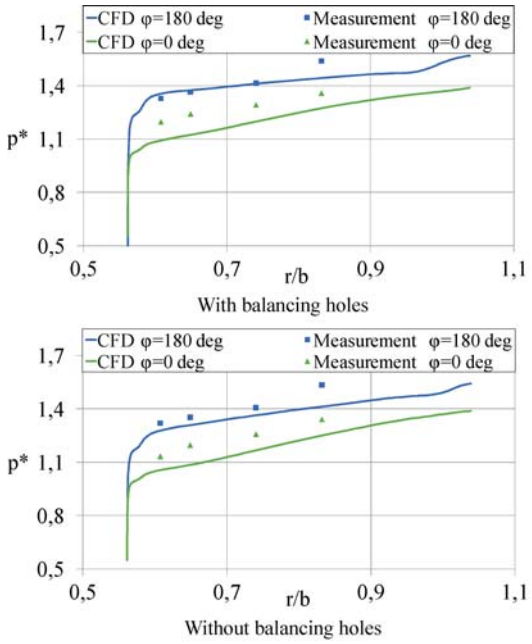

Fig. 11 Radial pressure distribution in the front impeller side clearances (Q/Qopt=0.6)

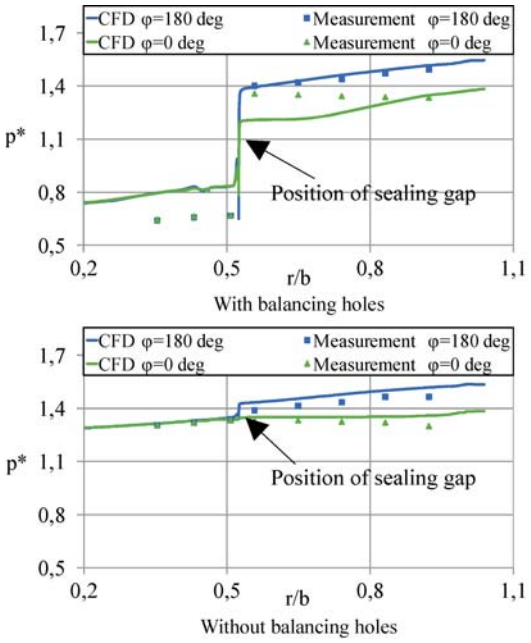

Fig. 12 Radial pressure distribution in the rear impeller side clearances (Q/Qopt=0.6)

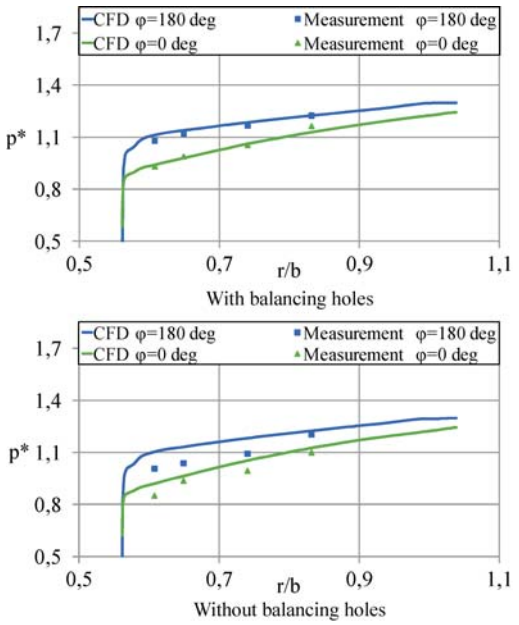

Fig. 13 Radial pressure distribution in the front impeller side clearances (Q/Qopt=1.2)

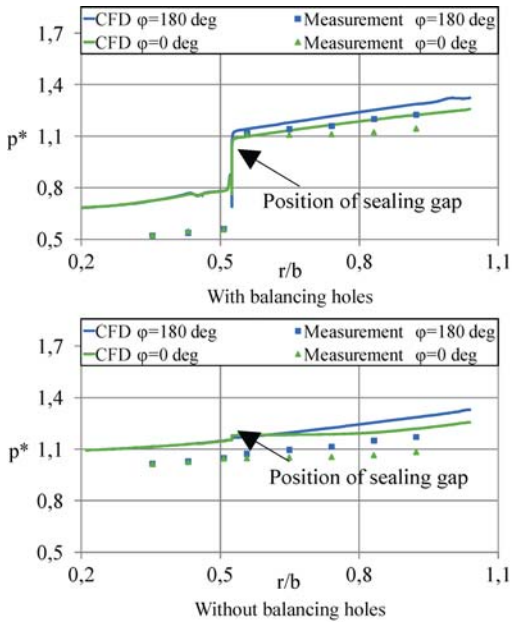

Fig. 14 Radial pressure distribution in the rear impeller side clearances (Q/Qopt=1.2)

flow field towards the suction side of the pump, which increases the net inward angular momentum flux. For this reason, the pressure drop in the front impeller side clearances increases.

The pressure distributions in the rear impeller side clearances allow the conclusion that flow regime III exists for all operating points whereas regime IV persists in the front impeller side clearances. Furthermore, the pressure distribution in case of overload without balancing holes shows that the pressure asymmetry diminishes for decreasing radial location. This is a consequence of the homogenizing effect of viscosity in the rear impeller side clearances.

Summary and Conclusions

Numerical simulations of a centrifugal pump with volute casing including the impeller side clearances are

used to predict the flow fields for three different operating points and two configurations of the impeller namely with and without balancing holes. Measurements of the radial static pressure distribution in both impeller side clearances at two different tangential positions are performed and compared to the numerical results. To determine the overall performance, the hydraulic head is measured as well. A close agreement for the hydraulic head is found in all configurations and operating points. In general, the pressure distribution in the front impeller side clearances agrees well with the numerical results. Somewhat larger deviations occur in the rear impeller side clearances. Due to the different gap widths, the flow structure in the impeller side clearances is inherently different. In the front impeller side clearances, the axial distance between the rotating and the stationary wall is large enough so that two boundary layers can develop on the rotating and the stationary wall. In the rear impeller side clearances, merged boundary layers are present due to the small axial gap width. Consequently, the pressure distributions obtained are quite dissimilar. This applies to all operating points investigated.

The flow in the impeller side clearances is strongly coupled with the flow in the volute and the impeller outflow. In the standard configuration, the impeller is equipped with balancing holes. Closing of these holes drastically changes the flow conditions in both impeller side clearances due to a totally different secondary flow field in the volute. More precisely, the inward angular momentum flux increases in the front impeller side clearances since more high energy fluid from the impeller is entrained.

In the investigated pump, the pressure in the volute changes in tangential direction even at design flow rate and consequently, in both impeller side clearances, too. For the impeller configuration without balancing holes, a recirculation pattern in the rear impeller side clearances develops as a direct consequence of the inhomogeneous pressure pattern. This demonstrates that the outer pressure field in the volute strongly dictates the flow conditions even in the narrow rear impeller side clearances. Since no recirculation region is found if the impeller is equipped with balancing holes, the presence of a radial flow component is expected to suppress the wake.

The proposed flow model yields good results for the radial pressure distribution in the front impeller side clearances, since the gap width obviously is large enough to allow for the formation of flow regime IV. In the rear impeller side clearances, a considerably smaller axial gap width prevents the formation of the so called Batchelor flow. For this reason, the flow in this region is strongly affected by viscous effects. As a result, the radial pressure drop is reduced and the shape of the curve is altered compared with the front impeller side clearances. Therefore, an approach proposed by [12] must be used to adequately calculate the radial pressure distribution. Both flow models incorporated emerge from the assumption of axi-symmetric flow conditions and can hence only yield an average estimation of the pressure distribution. However, the theoretical results fall right between the measured data at the two circumferential positions as long as sufficiently accurate boundary conditions are applied.

In conclusion, the flow structure in the impeller side clearances of a real machine is very complex and inseparably influenced by the interaction with the flow in the adjacent components. Analytical flow models for the impeller side clearances can yield reasonable results if accurate boundary conditions are provided. To determine these boundary values, the flow in the adjacent parts has to be taken into consideration as well.

Acknowledgements

The authors would like to thank Tobias Ecker, M.S. from Virginia Polytechnic Institute and State University for his assistance in preparing the final version of this paper.

References

[1] Will, B.C., Benra, F.K., Dohmen, H.J., 2010, Numerical and Experimental Investigation of the Flow in the Side Cavities of a Centrifugal Pump, The 12th International Symposium on Transport Phenomena and Dynamics of Rotating Machinery, ISROMAC13-2010-0002, Honolulu, Hawaii, USA.

[2] Daily, J.W., Nece, R.E., 1960, Chamber Dimension Effects on Induced Flow and Frictional Resistance of Enclosed Rotating Disks, Journal of Basic Engineering, 82, p. 217–232.

[3] Daily, J.W., Ernst, W.D., Asbedian, V.V., 1964, Enclosed Rotating Disks with Superposed Throughflow, Massachusetts Institute of Technology, Report No. 64, Boston.

[4] Hamkins, C.P., 1999, The Surface Flow Angle in Rotating Flow: Application to the Centrifugal Pump Impeller Side Gap, Dissertation, TU Kaiserslautern, Kaiserslautern.

[5] Gülich, J.F., 2010, Handbuch Kreiselpumpen, Springer-Verlag, Berlin, Germany.

[6] Senoo, Y., Hayami, H., 1976, An Analysis on the Flow in a Casing Induced by a Rotating Disk Using a Four-Layer Flow Model, Transactions of the ASME, Journal of Fluids Engineering, p. 192–198.

[7] Bennet, T.P., Worster, R.C., 1961, The Friction on Rotating Disc and Effect on Net Radial Flow and Externally Applied Whirl, British Hydromechanics Research Association, Cranfield, Bedford, Report RR691.

[8] Will, B.C., Benra, F.K., 2009, Investigation of the Fluid Flow in a Rotor-Stator Cavity with Inward Through-Flow, Proceedings of FEDSM2009, ASME Fluids Engineering Conference, FEDSM2009-78503, Vail, Colorado, USA.

[9] Truckenbrodt, E., 1989, Fluidmechanik, Springer-Verlag, Heidelberg, Germany.

[10] Poncet, S., Chauve, M.P., Le Gal, P., 2005, Turbulent Rotating Disk Flow with Inward Through-Flow, Journal of Fluid Mechanics, Vol. 522, p. 253–262.

[11] Kurokawa, J., Toyokura, T., 1972, Study on Axial Thrust of Radial Flow Turbomachinery, The second International JSME Symposium Fluid Machinery and Fluidics, Tokyo, p. 31–40.

[12] Kurokawa, J., Sakuma, M., 1988, Flow in a Narrow Gap along an Enclosed Rotating Disk with Through-Flow, JSME International Journal, Series II, Vol. 31, No.2, p. 243–251.

[13] Schultz-Grunow, F., 1935, Der Reibungswiderstand rotierender Scheiben in Gehäusen, Zeitschrift für angewandte Mathematik und Mechanik, 15, p. 191–204.

[14] Poncet, S., Schiestel, R., Chauve, M.P., 2005, Turbulence Modelling and Measurements in a Rotor-Stator System with Throughflow, Engineering Turbulence Modelling and Measurements, ETMM6, Sardinia, Italy, Ed. W. Rodi & M. Mulas, Elsevier, p. 761–770.

[15] Lauer, J., 1999, Einfluss der Eintrittsbedingung und der Geometrie auf die Strömung in den Radseitenräumen von Kreiselpumpen, Dissertation, TU Darmstadt, Darmstadt.

[16] Radtke, F., Ziemann, M., 1983, Experimentelle und theoretische Untersuchungen des Reibungseinflusses an rotierenden Scheiben, Forschungsvereinigung Verbrennungskraftmaschinen e.V., (FVV) - Forschungsberichte No. 331, Frankfurt.

[17] Möhring, U.K., 1976, Untersuchung des radialen Druckverlaufes und des übertragenen Drehmomentes im Radseitenraum von Kreiselpumpen bei glatter, ebener Radseitenwand und bei Anwendung von Rückenschaufeln, Dissertation, TU Braunschweig, Braunschweig.

[18] Poncet, S., Da Soghe, R., Facchini, B., 2010, RANS modeling of flows in rotating disk systems, V European Conference on Computational Fluid Dynamics, ECCOMAS CFD 2010, Lisbon, Portugal.